Bull. Natl. Mus. Nat. Sci., Ser. C, 51, pp. 1–8, December 19, 2025

DOI: 10.50826/bnmnsgeopaleo.51.0_1

Holtstamite from the Chichibu Mine, Japan, and Its Compression Behavior

Daisuke Nishio-Hamane[1]*, Koichi Momma[2] and Akira Harada[3]

[1] Institute for Solid State Physics, the University of Tokyo, Kashiwa, Chiba 277–8581, Japan
[2] Department of Science, the National Museum of Nature and Science, Tsukuba, Ibaraki 305–0005, Japan
[3] Midorigaoka, Chuo-ku, Sagamihara City, Kanagawa 252–0225, Japan
Author for correspondence: hamane@issp.u-tokyo.ac.jp

Abstract Holtstamite was discovered in large quantities as a rock mass in the Sekkaizawa of the Chichibu mine, Saitama Prefecture, Japan. This report presents the first documented occurrence of holtstamite in Japan, as well as the first evidence of its distribution on a rock-unit scale. It also provides the first experimental insight into the high-pressure compression behavior of holtstamite. Holtstamite is Mn^{3+}-free to show the nearly end-member composition of $(Ca_{2.85}Mg_{0.13})_{\Sigma 2.98}(Al_{1.87}Fe_{0.06})_{\Sigma 1.93}Si_{2.06}O_8(OH)_4$. The unit-cell parameters refined by the Rietveld method are a = 12.1611(13), c = 11.9682(13) Å, V = 1770.0(3) Å^3, and Z = 8 in conjunction with the $I4_1/acd$ space group, indicating that tetragonal symmetry is an intrinsic feature of the crystal structure of holtstamite even in the Mn^{3+}-free system. The third-order Birch–Murnaghan equation of state yields K_0 = 104.5(8) GPa and K_0' = 4.29(5), and the second-order Birch–Murnaghan equation of state yields K_0 = 108.8(3) GPa. The systematics of the bulk modulus clearly indicate that the degree of hydrous component is the dominant factor in the overall compressibility. Under the high pressure, the tetragonal distortion is gradually eliminated, but the rate is slower at 3-6 GPa and remains unchanged above 6 GPa. Considering the high-pressure transition of katoite, a completely hydrated garnet, axial behavior in holtstamite is thought to be the result of a gradual strengthening of H–H repulsion.

Key words: holtstamite, henritermierite, high pressure, Chichibu mine

Introduction

Holtstamite, ideally $Ca_3Al_2(SiO_4)_2(OH)_4$, is an independent mineral species of the garnet supergroup, with intermediate composition (x = 1) between grossular (x = 0) and katoite (x = 3) as $Ca_3Al_2(SiO_4)_{3-x}(H_4O_4)_x$ (Grew *et al.*, 2013). Holtstamite in the first report contained a large amount of Mn^{3+} and has also tetragonal symmetry with the $I4_1/acd$ space group, while grossular and katoite show cubic symmetry of the $Ia\bar{3}d$ space group. Thus, Hålenius *et al.* (2005) suggest that the Jahn–Teller cation Mn^{3+} is necessary to stabilize the tetragonal distortion. On the other hand, this study found holtstamite that was Mn^{3+}-free composition but maintained the tetragonal symmetry.

Katoite, a typical model mineral of the Si^{4+}–$4H^+$ substitution, has attracted great interest in its behavior under high pressure (Olijnyk *et al.*, 1991; Lager and VonDreele, 1996; Lager *et al.*, 2002; Lager *et al.*, 2005; Kyono *et al.*, 2019; Kato and Kyono, 2019). Until now, holtstamite was thought to occur only in trace amounts, but it has been discovered to occur in large quantities as a rock mass in this study. Thus, the high-pressure behavior of holtstamite should be as important as that of katoite. The high-pressure behavior of henritermierite, a tetragonal hydrous garnet that is a Mn^{3+}-dominant analogue of holtstamite, has been reported previously (Armbruster *et al.*, 2001), and comparison with this may also facilitate understanding of the high-pressure behavior of the garnet group.

This study presents the first report of holtstamite from Japan, as well as the first documented occurrence of it on a rock-unit scale. It also marks the first experimental investigation of the high-pressure compression behavior of holtstamite. In this study, we briefly summarize the description of holtstamite and then report the compression behavior of the natural sample up to about 10 GPa using a diamond anvil cell. The rock sample (NSM-047616) and thin section (NSM-047615) have been deposited in the collection of the National Museum of Nature and Science, Japan.

Mineral description

Occurrence

The Chichibu mine is located approximately 25 km west of Chichibu city in Saitama Prefecture, Japan, where several typical skarn-type deposits are developed. The entrance to the Sekkaizawa valley lies about 1 km northeast of the mine office, and the valley extends eastward upstream (36°01′02″N 138°48′50″E). Within this area, three major limestone bodies have been identified; the largest of these was designated the "second limestone body" by Katayama *et al.* (1954). In our observation, skarns associated with the second limestone body can be classified into several types, including andradite-, vesuvianite-, spinel-, gehlenite-, and holtstamite-rich skarns. These occur sporadically along the southern slope of Sekkaizawa at elevations between 1050 and 1150 m.

The gehlenite-rich skarn, which corresponds to a high-temperature skarn, is distributed over a limited area approximately 5 m wide and 1.5 m high. Approximately 30 m east of this exposure, a holtstamite-rich skarn was found, extending across a horizontal span of 3 m and a vertical span of 1.5 m. Further east, small outcrops of spinel- and vesuvianite-rich skarns are present.

The holtstamite rock shows white in color, while the parts containing a lot of amesite show bluish gray in color. This rock also contains small aggregates of vesuvianite and chantalite (Fig. 1). The mineral grains composed of holtstamite are up to 500 µm in size but are spongy and consist of aggregate of microcrystals (Fig. 2). Since the gehlenite rock with vesuvianite inside is exposed in close proximity to the holtstamite rock, holtstamite were probably formed by alteration of gehlenite.

Fig. 1. The photograph of the rock sample mainly composed of holtstamite collected at the Sekkaizawa. Holtstamite (Hts), amesite (Ame), vesuvianite (Ves), and chantalite (Cht).

Chemical composition

The chemical composition of the holtstamite was determined by a JEOL IT-100 (SEM-EDS mode, 15 kV, 0.8 nA, 1 µm beam diameter, the ZAF correction). The amount of Mn was below the detection limit (0.1 wt% in Mn_2O_3). The sample is homogeneous throughout the rock specimen and shows very little compositional variation both between individual grains and within each grain. Analytical data from 20 separate grains across four thin sections yielded standard devia-

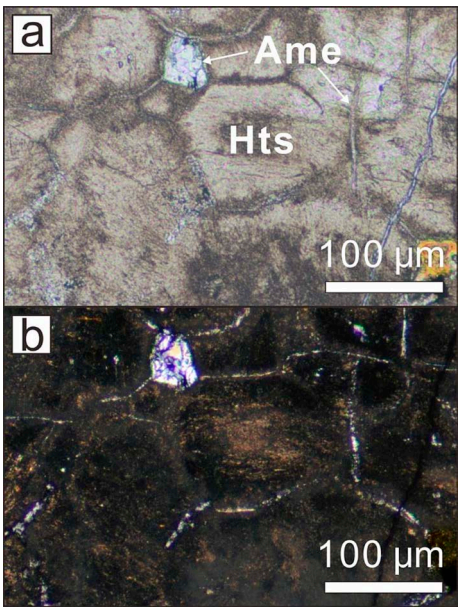

Fig. 2. Photomicrographs of holtstamite (Hts) with amesite (Ame) taken under plane-polarized light (a) and cross-polarized light (b).

Table 1. Chemical composition of holtstamite.

	wt% (n = 20)					apfu
	Avg.	Min.	Max	S.D.*	Ca	2.85
CaO	37.28	35.41	38.53	0.80	Mg	0.13
MgO	1.26	0.57	2.64	0.54	Σ	2.98
Al_2O_3	22.21	21.09	23.50	0.64		
Fe_2O_3	1.14	0.69	1.70	0.30	Al	1.87
SiO_2	28.80	28.11	29.22	0.30	Fe	0.06
H_2O**	8.39				Σ	1.93
Total	99.08					
					Si	2.06
					O =	8
					OH =	4

* Standard deviation
** Calculation as OH = 4

tions of less than 1 wt% for each oxide (Table 1). The empirical formula of holtstamite based on the O = 8 and OH = 4 atoms per formula unit (apfu) is $(Ca_{2.85}Mg_{0.13})_{\Sigma 2.98}(Al_{1.87}Fe_{0.06})_{\Sigma 1.93}Si_{2.06}O_8(OH)_4$, which is considerably close to the end-member composition $Ca_3Al_2(SiO_4)_2(OH)_4$ (Table 1).

X-ray crystallography

The crystal structure refinement of holtstamite was carried out using the Rietveld method implemented in RIETAN-FP by Izumi and Momma (2007), because it was an aggregate of microcrystals. The powder X-ray diffraction (XRD) pattern was obtained using a Gandolfi camera (114.6 mm in diameter, Ni-filtered Cu$K\alpha$ radiation at 30 kV, 20 mA). The exposure time was 96 hours. A two-dimensional X-ray diffraction image was integrated with respect to 2θ (the range of 15–130° with 0.025° step) to obtain 2θ-intensity XRD profiles using a computer program written by Nakamuta (1999). A pseudo-Voigt profile function by Thompson *et al.* (1987) in combination of peak asymmetry function by Finger *et al.* (1994) and a background function of Legendre polynomials with 11th order were used in the refinement. A small amount of amesite contamination is inevitable due to the occurrence, and thus refinement was demonstrated as the two phases model of holtstamite with amesite. On the other hand, the amount of amesite is only minor, so its structure model was fixed in the one by Anderson and Bailey (1981) and only the scale factor was adjusted accordingly.

The structural formula as the tetragonal garnet in conjunction with the $I4_1/acd$ space group is $X1_2X2Y1_2Z1_2Z2O1_4O2_4(O3H1)_4$, and the structure was refined as an end-member composition, with only the occupancy of the $Z2$ site varied. The initial structure model of holtstamite was taken from Hålenius *et al.* (2005). The refinement of the Si occupancy at the $Z2$ site reveals that there is almost no Si at that site due to Si^{4+}–$4H^+$ substitution. The atomic displacement parameters were treated as common between X sites, between Y and Z sites, and between O sites. The H positions were fixed to

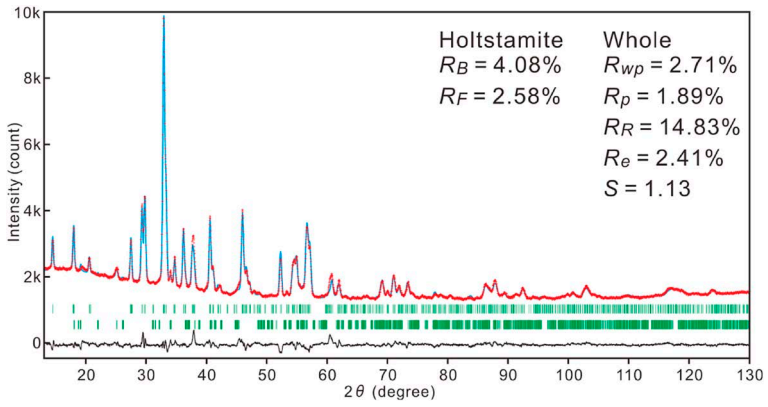

Fig. 3. Observed X-ray diffraction pattern (red crosses) and simulated pattern by the Rietveld refinement (solid blue line). Their residuals are given in bottom (black solid line). The green bars show the diffraction positions of holtstamite (the upper row) and amesite (the lower row), respectively.

Table 2. Refined atomic positions, site occupancies, and atomic displacement param for holtstamite*.

Site	Atom	Occupancy	x	y	z	B (Å^2)
$X1$	Ca	1	0.3700(3)	0	0.25	1.47(5)
$X2$	Ca	1	0	0.25	0.125	= $X1$
$Y1$	Al	1	0	0	0	1.17(5)
$Z1$	Si	1	0.1195(4)	0	0.25	= $Y1$
$Z2$	Si	0.06(6)	0.5	0.25	0.125	= $Y1$
$O1$	O	1	0.2897(3)	0.7134(4)	0.1004(5)	0.44(7)
$O2$	O	1	0.1516(5)	0.5441(4)	0.0467(3)	= $O1$
$O3$	O	1	0.4481(4)	0.3558(4)	0.0256(3)	= $O1$
$H1$	H	1	0.453	0.333	0.082	1

$I4_1/acd$, a = 12.1611(13) Å, c = 11.9682(13) Å, V = 1770.0(3) Å, and Z = 8.

*Estimated standard deviations are given in parentheses and values without standard deviations were fixed in the calculation.

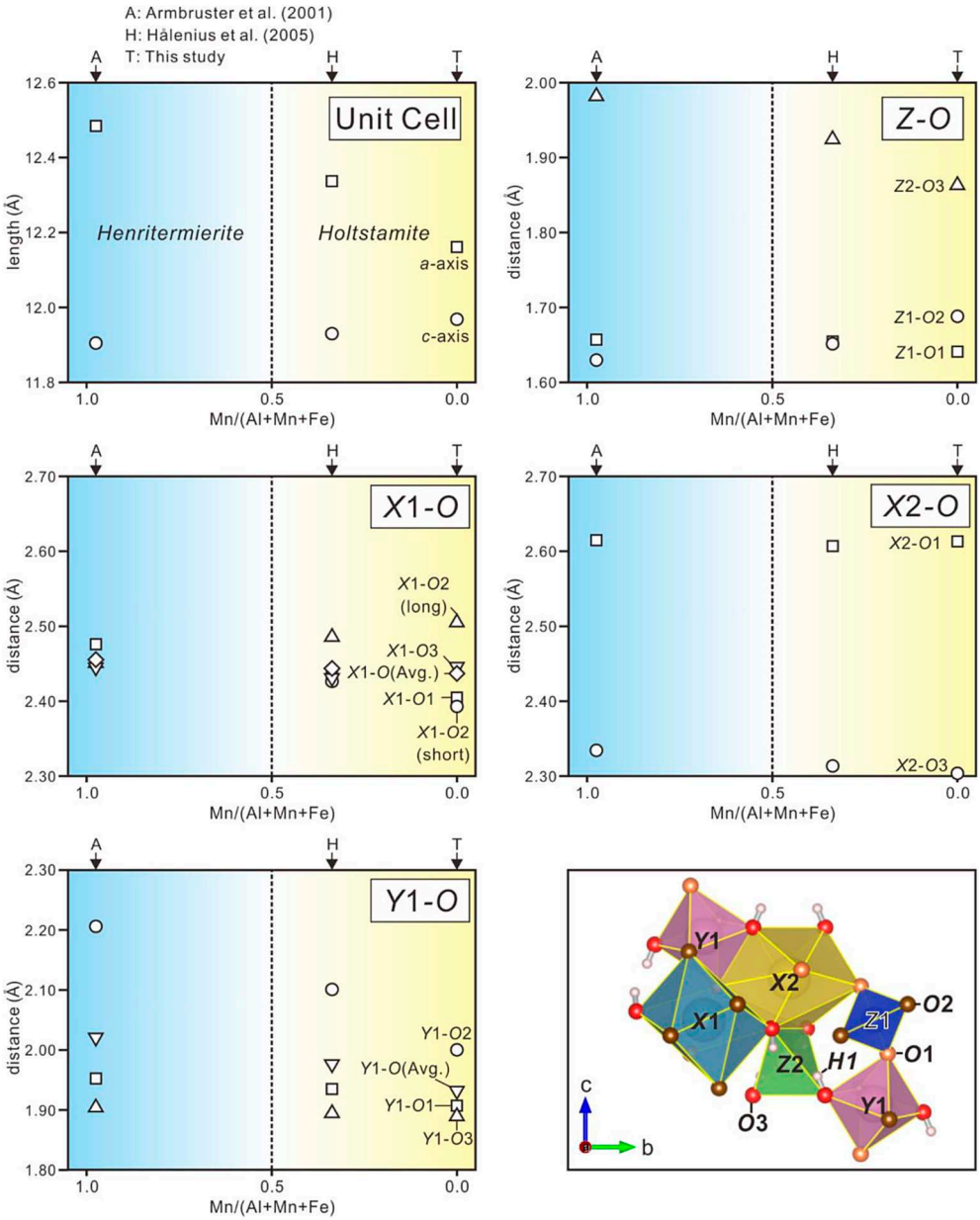

Fig. 4. Comparisons of the unit cell param, inter atomic distances, and crystal structure between holtstamite and henritermierite series.

the values in Hålenius *et al.* (2005). The R_{wp} converged into 2.71%, and the R_B and R_F of holtstamite converged into 4.08% and 2.58%, respectively (Fig. 3). The refined unit-cell parameters were a = 12.1611(13), c = 11.9682(13) Å, V = 1770.0(3) Å^3, and Z = 8. The refined parameters are summarized in Table 2.

Structural implications

Fig. 4 shows the relationship of the amount of Mn^{3+}, the tetragonal distortion, and internal interatomic distance. With increasing Mn^{3+}, the *a*-axis length increases and the *c*-axis length decreases, resulting in an increase in the tetragonal distortion. The *Y*1-O octahedron that accommodates Mn^{3+} has the characteristic that the *Y*1-*O*2 distance is longer, and the *Y*1-*O*1 and *Y*1-*O*3 distances are shorter in the Mn^{3+}-free composition, and this characteristic is significantly accentuated with the increase in Mn^{3+}. The average *Y*1-*O* distance increases by increasing Mn^{3+}, which has an ionic radius larger than Al^{3+} and Fe^{3+}. With increasing Mn^{3+}, the *Z*2-*O*3 distance increases and the *Z*1-*O*2 distance decreases, but the *Z*1-*O*1 distance remains unchanged. The *X*2-*O* distance also shows almost no fluctuation. The *X*1-*O* distance is clearly more scattered in the absence of

Mn^{3+} and rather converges as Mn^{3+} is increased. However, the average value of the *X*1-*O* distance does not fluctuate.

Conclusively, the present sample of holtstamite clearly retains tetragonal symmetry even in Mn^{3+}-free system. This is contrary to the suggestion by Hålenius *et al.* (2005) that Mn^{3+} is necessary for stabilizing tetragonal symmetry. Considering the results of our study, it is reasonable that tetragonal symmetry is an intrinsic feature of the crystal structure of holtstamite, and the role of Mn^{3+} is to promote the tetragonal distortion by largely increasing the distortion of the *Y*1-*O* octahedron.

High-pressure behavior

Method

Holtstamite with a composition consistent with the data in Table 1 was used in the experiment. It was ground into a powder and mixed with a fine gold powder as a pressure calibrant. High pressures were generated using a diamond anvil cell with 350 μm culet cut diamonds. The sample was loaded into 100 μm hole in the pre-compressed rhenium gasket together with a 4 : 1 methanol-ethanol mixture as hydrostatic pressure-transmitting medium. Angle-dispersive X-ray diffraction measurements were conducted at the NE1 beamline at the Photon Factory Advanced Ring (PF-AR) of KEK, Japan. This beamline provides a collimated beam (50 μm in diameter) of monochromatic synchrotron X-ray radiation (wavelength: 0.4177 Å). The XRD spectra were collected using the Debye-Scherrer method through the diamond anvil cell containing the sample and recorded via an imaging plate detector. The sample-to-detector distance and inclination of the detector were calibrated using standard material (CeO_2) at 1 atm. Exposure time was 10 minutes. A two-dimensional X-ray diffraction image was integrated with respect to 2θ (the range of 3–20° with 0.01° step) to obtain 2θ-intensity XRD profiles using IPAnalyzer by Seto *et al.* (2010).

Result and discussion

The powder XRD patterns were measured at 20 points from ambient pressure to 10 GPa (Table 3). Representative XRD patterns are shown in Fig. 5. The XRD patterns show some minor peaks of amesite and vesuvianite, while the major peaks were holtstamite and gold as pressure marker. The XRD pattern shifted to a higher angle with increasing pressure, but no drastic changes, such as the appearance or disappearance of peaks, occurred up to 10 GPa. The XRD pattern of holtstamite could still be indexed in the tetragonal system even at 10 GPa. As a result, the volume decreased with increasing pressure without any discontinuity or stagnation (Fig. 6a). Thus, the data were fitted using the third-order Birch–Murnaghan equation of state, as given by

$$P = 3/2K_0[(V/V_0)^{-7/3} - (V/V_0)^{-5/3}] \{1 + 3/4(K_0' - 4)[(V/V_0)^{-2/3} - 1]\} \quad (1)$$

where V_0 is the volume at zero pressure, K_0 is the isothermal bulk modulus and K_0' is the first pressure derivative of the isothermal bulk modulus. If we fix K_0' at 4, we obtain the second-order Birch–Murnaghan equation of state. Then, the third-order Birch–Murnaghan equation of state yields K_0 = 104.5(8) GPa and K_0' = 4.29(5), while the second-order Birch–Murnaghan equation of state yields K_0 = 108.8(3) GPa. The bulk modulus of holtstamite is roughly intermediate between those of grossular and katoite and is comparable to that of henritermierite (Table 4). The systematics of the bulk modulus clearly indicate that the degree of hydrous component is the dominant factor in the overall compressibility. Similarly, it was shown that the

Table 3. Unit cell parameters of holtstamite under high pressure.

P (GPa)	*a* (Å)	*c* (Å)	*V* (Å^3)
1 atm	12.171(3)	11.968(5)	1772.8(8)
0.63	12.145(3)	11.947(4)	1762.3(6)
1.06	12.128(3)	11.932(4)	1755.0(7)
1.50	12.111(3)	11.916(4)	1747.9(7)
2.09	12.092(3)	11.899(4)	1739.8(6)
2.77	12.066(3)	11.876(4)	1729.1(7)
3.12	12.056(3)	11.867(4)	1724.7(6)
3.98	12.026(3)	11.838(4)	1712.2(7)
4.50	12.012(3)	11.825(4)	1706.1(7)
5.18	11.991(3)	11.805(4)	1697.3(7)
6.24	11.956(3)	11.771(4)	1682.5(7)
6.46	11.948(3)	11.763(4)	1679.1(8)
6.85	11.937(3)	11.754(4)	1674.9(7)
7.45	11.921(3)	11.738(4)	1668.1(7)
7.87	11.909(3)	11.725(4)	1662.8(7)
8.56	11.890(3)	11.707(4)	1655.1(7)
9.12	11.877(3)	11.695(4)	1649.8(7)
9.16	11.875(3)	11.692(4)	1648.8(7)
9.68	11.863(3)	11.681(4)	1643.8(7)
10.00	11.854(3)	11.672(4)	1640.0(7)

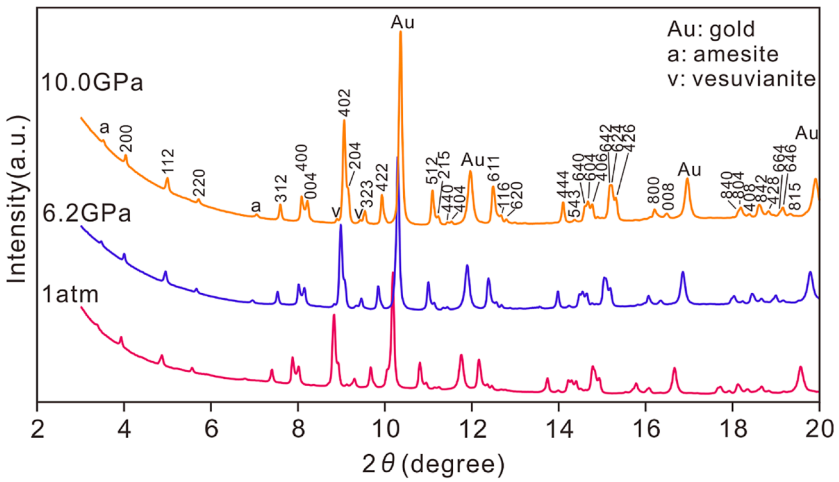

Fig. 5. The representative XRD patterns of holtstamite under the high pressure. The numbers above diffraction profile are the Miller indices for holtstamite.

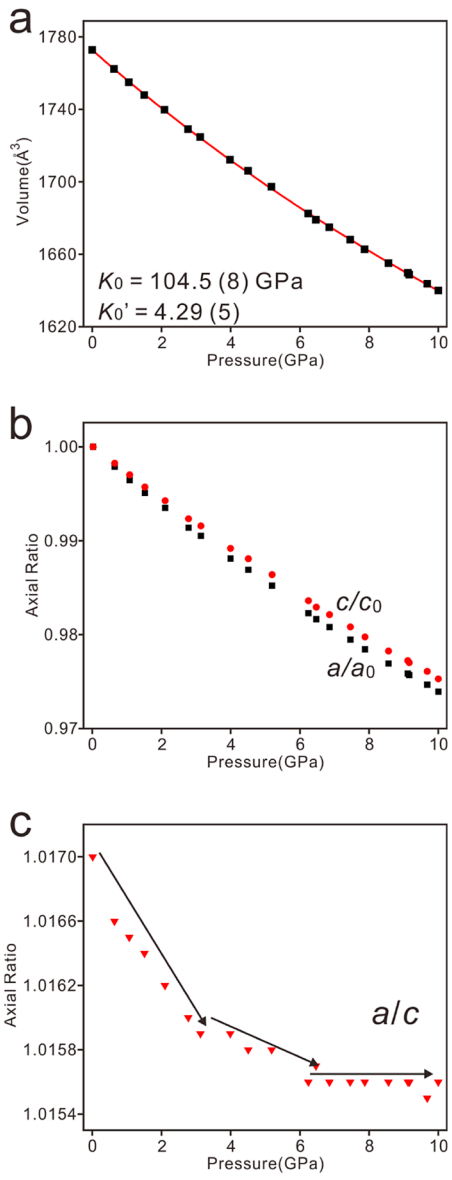

Fig. 6. Compression behavior of unit cell volume (a), each axis (b), and axial ratio (c).

degree of Al–Mn substitution has an insignificant effect on the compressibility in tetragonal hydrogarnet. On the other hand, holtstamite shows remarkably smaller K_0' than in henritermierite ($K_0' = 5.3$) (Armbruster *et al.*, 2001), suggesting that Al-Mn substitution may affect K_0' rather than K_0.

Focusing on the lengths of *a*-axis and *c*-axis, a/a_0 was always smaller than c/c_0 in holtstamite under the pressure (Fig. 6b). This indicates that the originally longer *a*-axis is more compressible than the *c*-axis, which results in the relaxation of tetragonal distortion. However, the release of distortion is not constant (Fig. 6c). The distortion is released gradually up to about 3 GPa, but in the range of 3–6 PGa, the release seems to be slower than before. Above 6 GPa, no strain release is observed at all. In katoite, it is known that the H–H repulsion triggers to occur a phase transition under pressure of approximately 5 GPa (Lager *et al.*, 2002; Kato and Kyono, 2019). Similarly, the variation in *a*/*c* in holtstamite at 3–6 GPa may indicate the onset of H–H repulsion, and the constant *a*/*c* above 6 GPa may mean that the repulsion becomes even stronger.

Nevertheless, such behavior has not been observed in henritermierite. Even at the same pressure, the tetragonal distortion of henritermierite remains more firmly than that of holtstamite, and the strain release was more abrupt and continuous (Armbruster *et al.*, 2001). This is probably because the influence of the Jahn-Teller effect of Mn^{3+} is much notable in henritermierite, and the H–H distance is not short enough to cause repulsion. Although tetragonal distortions remain in holtsta-

Table 4. Comparison of bulk modulus between representative garnets.

Mineral	Ideal composition	K_0 (GPa)	K_0'	Reference
Grossular	$Ca_3Al_2(SiO_4)_3$	166	4(fixed)	1
		170	5.2	2
		171.2	4.47	3
Holtstamite	$Ca_3Al_2(SiO_4)_2(OH)_4$	108.8(3)	4(fixed)	4
		104.5(8)	4.29(5)	
Henritermierite	$Ca_3Mn^{3+}{}_2(SiO_4)_2(OH)_4$	98	5.3	5
Katoite	$Ca_3Al_2(OH)_{12}$	58	4.0	6
		52	4(fixed)	7

1, Gréaux *et al.* (2011); 2, Zhang *et al.* (1999); 3, Gwanmesia *et al.* (2014); 4, This study; 5, Armbruster *et al.* (2001); 6, Lager *et al.* (2002); 7, Lager and von Dreele (1996).

mite under high pressure, the lengths of the *a*- and *c*-axes are comparable that there should be little difference in the H–H distance no matter which direction the H site is located. On the other hand, in henritermierite, H may be located in the *a*-axis direction, where repulsion is less likely to occur, owing to large tetragonal distortion due to the Jahn-Teller effect of Mn^{3+}. However, it is not easy to determine the H position with small scattering factors, and the H site has not been identified. Further investigation for the H position under high pressure is required in both holtstamite and henritermierite in the feature.

Conclusion

Mn^{3+}-free holtstamite was discovered from the Sekkaizawa in the Chichibu mine, Saitama Prefecture, Japan. Holtstamite can maintain tetragonal symmetry even in Mn^{3+}-free composition. This result makes the role of Mn^{3+} more concrete. In other words, tetragonal symmetry is an essential feature of the crystal structure of holtstamite, and the role of Mn^{3+} is to promote tetragonal distortion by greatly increasing the octahedral distortion through the Jahn-Teller effect.

The compression behavior under high pressure clearly indicates that the degree of the hydrous component is the dominant factor in overall compressibility. Under high pressure, the H-H repulsion can occur in holtstamite, as in katoite, but not in henritermierite, Mn^{3+} analogue of holtstamite. Further studies are needed to determine the location of H under high pressure in both holtstamite and henritermierite.

Acknowledgement

The synchrotron X-ray diffraction data were acquired at KEK (Proposal no. 2017G584).

References

Anderson, C. S. and Bailey, S. W. (1981) A new cation ordering pattern in amesite-2H2. *American Mineralogist*, **66**: 185–195.

Armbruster, T., Kohler, T., Libowitzky, E., Friedrich, A., Miletich, R., Kunz, M., Medenbach, O. and Gutzmer, J. (2001) Structure, compressibility, hydrogen bonding, and dehydration of the tetragonal Mn^{3+} hydrogarnet, henritermierite. *American Mineralogist*, **86**: 147–158.

Finger, L. W., Cox, D. E. and Jephcoat, A. P. (1994) A correction for powder diffraction peak asymmetry due to axial divergence, *Journal of Applied Crystallography*, **27**: 892–900.

Gwanmesia, G. D., Wang, L., Heady, A. and Liebermann, R. (2014) Elasticity and sound velocities of polycrystalline grossular garnet ($Ca_3Al_2Si_3O_{12}$) at simultaneous high pressures and high temperatures. *Physics of the Earth and Planetary Interiors*, **228**: 80–87.

Gréaux, S., Nishiyama, N., Kono, Y., Gautron, L., Ohfuji, H., Kunimoto, T., Menguy, N. and Irifune, T. (2011) Phase transformations of $Ca_3Al_2Si_3O_{12}$ grossular garnet to the depths of the Earth's mantle transition zone. *Physics of the Earth and Planetary Interiors*, **185**: 89–99.

Grew, E. S., Locock, A. J., Mills, S. J., Galuskina, I. O., Galuskin, E. V. and Hålenius, U. (2013) Nomenclature of the garnet supergroup. *American Mineralogist*, **98**: 785–811.

Hålenius, U., Haussermann, U. and Harryson, H. (2005) Holtstamite, $Ca_3(Al,Mn^{3+})_2(SiO)_4)_{3-x}(H_4O_4)_x$, a new tetragonal hydrogarnet from Wessels Mine, South Africa. *European Journal of Mineralogy*, **17**: 375–382.

Izumi, F. and Momma, K. (2007) Three–dimensional visualization in powder diffraction. *Solid State Phenomena*, **130**: 15–20.

Katayama, N., Takano, Y., Kato, I., Kato, T. and Nakagawa, S. (1954) Occurrence of scarn minerals at Hashikakezawa, Sekkai-zawa and Deai in the Chichibu mine. *Journal of the Mineralogical Society of Japan*, **2**: 46–52.

Kato, M. and Kyono, A. (2019) An in situ Raman study on katoite $Ca_3Al_2(O_4H_4)_3$ at high pressure. *Journal of*

Mineralogical and Petrological Sciences, **114**: 18–25.

Kyono, A., Kato, M., Sano-Furukawa, A., Machida, S. and Hattori, T. (2019) Crystal structure change of katoite, $Ca_3Al_2(O_4D_4)_3$, with temperature at high pressure. *Physics and Chemistry of Minerals*, **46**: 459–469.

Lager, G. A. and Von Dreele, R. B. (1996) Neutron powder diffraction study of hydrogarnet to 9.0 GPa. *American Mineralogist*, **81**: 1097–1104.

Lager, G. A., Downs, R. T., Origlieri, M. and Garoutte, R. (2002) High-pressure single-crystal X-ray diffraction study of katoite hydrogarnet: Evidence for a phase transition from $Ia3d \rightarrow I4\bar{3}d$ symmetry at 5 GPa. *American Mineralogist*, **87**: 642–647.

Lager, G. A., Marshall, W. G., Liu, Z. X. and Downs, R. T. (2005) Re-examination of the hydrogarnet structure at high pressure using neutron powder diffraction and infrared spectroscopy. *American Mineralogist*, **90**: 639–644.

Nakamuta, Y. (1999) Precise analysis of a very small mineral by an X-ray diffraction method. *Journal of the Mineralogical Society of Japan*, **28**: 117–121 (in Japanese with English abstract).

Olijnyk, H., Paris, E., Geiger, C. A. and Lager, G. A. (1991) Compressional study of katoite $[Ca_3A1_2(O_4H_4)_3]$ and grossular garnet. *Journal of Geophysical Research*, **96(B9)**: 14313–14318.

Thompson, P., Cox, D. E. and Hastings, J. B. (1987) Rietveld refinement of Debye-Scherrer synchrotron X-ray data from Al_2O_3, *Journal of Applied Crystallography*, **20**: 79–83.

Seto, Y., Nishio–Hamane, D., Nagai, T. and Sata, N. (2010) Development of a software suite on X–ray diffraction experiments. *The Review of High Pressure Science and Technology*, **20**: 269–276 (in Japanese with English abstract).

Zhang, L., Ahsbahs, H., Kutoglu, A. and Geiger, A. A. (1999) Single-crystal hydrostatic compression of synthetic pyrope, almandine, spessartine, grossular and andradite garnets at high pressures. *Physics and Chemistry of Minerals*, **27**: 52–58.